154 (2026) 205966

Contents lists available at ScienceDirect

Gas Science and Engineering

journal homepage: www.journals.elsevier.com/gas-science-and-engineering

A hybrid-EoS approach for multiphase pressure-based equilibrium calculations of reservoir mixtures with brine

M. Wapperom [a], J. Heringer [b], D.V. Nichita [b], D. Voskov [a,c,*]

[a] Department of Geoscience & Engineering, Delft University of Technology, Stevinweg 1, Delft, 2628 CN, Netherlands
[b] Laboratoire des Fluides Complexes, Université de Pau et des Pays de l'Adour, Pau Cedex, 64013, France
[c] Department of Energy Science & Engineering, School of Earth Sciences, Stanford University, 367 Panama Street, Stanford, 94305, CA, United States

ARTICLE INFO

Keywords:
Multiphase equilibrium
Equations of state
Aqueous phase
Fugacity-activity
Isothermal
Isenthalpic
Isentropic

ABSTRACT

Mixtures containing different gases, liquid hydrocarbons and aqueous brines play a very important role in modern energy transition applications. Cubic equations of state have proven reliable for thermodynamic calculations of nonpolar mixtures, but in their conventional form, they are not adequate to predict the interaction between associating molecules and fail to describe the behaviour close to infinite dilution. In this work, we develop an approach for combining thermodynamic models to represent different phase types thereby overcoming this inaccuracy. A cubic equation of state is used for non-aqueous phases, while a separate thermodynamic model is employed for the brine, combining Henry's constants for solutes and a fugacity model for the water component. In this way, we can maintain the computational efficiency of cubic EoS while modelling properties of the aqueous phase with good accuracy. We distinguish the vapour- and liquid-like roots of the cubic equation of state to correctly identify the minima of the Gibbs free energy surfaces in water-rich compositions. The use of different thermodynamic models introduces a thermodynamic inconsistency that is most noticeable close to the critical conditions of the water phase. However, the approach is valid and particularly accurate far from critical conditions for brine systems. The validity of the method up to these conditions is proven. Within these ranges, the proposed approach outperforms a setup using an association model (CPA EoS) both in terms of accuracy and performance. For optimal use in simulation, we present a framework for modelling multiphase equilibria involving reservoir mixtures with brine, which can be formulated at any pressure-based state specification. We validate the approach by comparing our phase equilibrium calculations with an experimental dataset of gas mixtures with water, relevant to subsurface energy transition applications.

1. Introduction

The transition to a carbon-neutral energy supply relies heavily on the development of subsurface technologies, such as geothermal energy production, geological CO_2 sequestration, and hydrogen storage. The successful implementation of these processes heavily depends on the accuracy and robustness of the procedures that model the underlying chemical and physical phenomena. The abundance of aqueous brine in target reservoirs for subsurface applications requires careful thermodynamic modelling of mixtures involved in the different stages of the operation cycle, the behaviour of brines being highly dependent on their composition. For the simulation of these processes, an accurate evaluation of the aqueous phase properties to capture its interaction with other reservoir and injected fluids is therefore necessary.

Classic van der Waals-type equations of state (EoS), such as SRK (Soave, 1972) and PR EoS (Peng and Robinson, 1976), have proven reliable for thermodynamic calculations of non-polar mixtures. By their cubic nature, the efficiency of these EoSs is unparallelled. Yet, in their conventional form, they are not adequate for mixtures of like and unlike molecules, as is the case in aqueous mixtures. In aqueous solutions, the presence of hydrogen-bonded clusters yields very different molecular and bulk fluid properties from nonpolar mixtures. This association results in structure formation between water molecules and around solutes. Cubic models have an attractive and a repulsive term, which together are not sufficient to predict the interaction between the associating molecules. Secondly, the models fail to describe the behaviour close to infinite dilution, at which solute–solvent interactions dominate. As a result, the prediction of gas solubilities in the aqueous phase using conventional mixing rules may deviate by orders of magnitude.

Modifications to the cubic equations of state have been proposed to improve phase behaviour prediction. Activity coefficient models can be

* Corresponding author at: Department of Geoscience & Engineering, Delft University of Technology, Stevinweg 1, Delft, 2628 CN, Netherlands.
E-mail address: d.v.voskov@tudelft.nl (D. Voskov).

https://doi.org/10.1016/j.jgsce.2026.205966
Received 7 August 2025; Received in revised form 25 May 2026; Accepted 22 June 2026
Available online 1 July 2026

applied to model equilibria in aqueous systems, however, they cannot easily account for the highly nonideal behaviour of aqueous solutions, and the adjustable parameters hold little physical significance. Alternatively, highly specific temperature-dependent or density-dependent binary interaction coefficients have been used to calculate the solubility of the gas in the water phase, an approach that has even been extended to the salinity dependence (Søreide and Whitson, 1992). However, it is not easy to accurately fit the temperature dependence for all phases. This forces one to combine different sets of parameters for different fluid types, which is not physically consistent. With density-dependent interaction parameters, quantitative agreement has been obtained for hydrocarbon solubilities, but the representation of the hydrocarbon phases is worse than that obtained with quadratic mixing rules (Michel et al., 1989).

A more theoretically sound approach for incorporating association and chain-forming into an equation was developed in the SAFT equations of state (Chapman et al., 1989). These models have additional terms and use statistical mechanical perturbation theory to quantify the relationship between molecular bonding site interactions and bulk fluid behaviour. Nonetheless, in spite of the increased complexity of the physical part of the EoS, the mutual solubilities of hydrocarbon–water systems are still very much dependent on the mixing rules used. This led to the development of the CPA EoS (Kontogeorgis et al., 1996), where the simple physical terms of a cubic equation of state have been combined with an association term similar to that used in the SAFT EoS. Yet, a significant drawback of using association models in pressure-based simulations is that they are explicit in volume, temperature and composition. While cubic equations of state are also volume-based, they can be solved for density analytically. In contrast, association terms are implicit and require iterative solutions for an internal set of composition-dependent variables (Michelsen and Hendriks, 2001).

Another approach is to use an entirely separate thermodynamic model for the aqueous phase. This approach introduces a thermodynamic inconsistency that is most pronounced near critical conditions. However, far from the critical conditions for brine systems (which is the case for the conditions of most depleted hydrocarbon fields and aquifers), the approach should still be applicable. An interesting feature of using a separate equation for the aqueous phase (and any other specific phase type) is the flexibility of modelling the properties of the aqueous phase irrespective of the restrictions of the other EoS.

Li and Nghiem (1986) presented multiphase equilibria for mixtures of oil and gas with water and brines based on Henry's constants for the aqueous phase. The nonaqueous fluids were modelled with a cubic equation of state, and Henry's coefficients were correlated against pressure and temperature. Models based on Henry's constants are essentially asymmetric activity-coefficient models, where the reference state is related to the solute–solvent interaction at infinite dilution. Considering the unlike nature of solvents and solutes, this is a more appropriate standard state to which solute thermodynamic properties are related. Furthermore, this approach to describe the dissolution of gases and hydrocarbons in the aqueous phase is justified, given their limited solubility. An important assumption when using Henry's constants is that in multicomponent systems, the interaction between solutes in solution is negligible. Evaluation of phase equilibria and aqueous equilibrium properties using such models at specified PT is rapid and accurate and therefore presents a good candidate for any multiphase P-based equilibrium calculations.

In this work, we develop an approach to combine equations of state to model different phase types in conventional phase-equilibrium calculations. The framework can be applied to any specific phase type, but we focus on the aqueous phase in particular. We use a cubic equation of state for the non-aqueous phases and a separate fugacity-activity model for the aqueous phase. In this model, the properties of dissolved gases are calculated from the approach of Ziabakhsh-Ganji and Kooi (2012). Their model combines Henry's constants for non-electrolyte solutes following Akinfiev and Diamond (2003). In addition, they included an additional term to account for the effect of brine salinity on gas solubilities, which was first proposed by Duan et al. (1992) and is based on excess Gibbs energies in electrolyte solutions (Pitzer, 1973). For the fugacity of the solvent (water), we follow the description of Jager et al. (2003). They derive the deviation of the chemical potential of H_2O from the pure water state, including the contributions of all molecular and ionic species to the water activity.

Using different thermodynamic models for different phases yields multiple minima of the Gibbs free energy surfaces in water-rich compositions and introduces inconsistencies towards the critical region of the brine phase. We illustrate these practical challenges through a Gibbs energy analysis and present strategies for implementing robust and efficient solution procedures. We validate the approach by comparing our phase equilibrium calculations using various pressure-based thermodynamic specifications with an experimental dataset of gas mixtures relevant to subsurface energy transition applications – CO_2, CH_4, H_2S and light hydrocarbons – with water. In addition, we demonstrate that the use of the hybrid-EoS approach is consistent and accurate for the evaluation of thermal properties, thus validating the extension of the framework for fast and accurate isenthalpic and isentropic flashes. Besides, the proposed approach was recently applied for modelling of hydrate formation and dissociation (Wapperom et al., 2026). While the models considered in this study have been extensively validated with experimental data for binary systems of water or brines with a single solute at moderate temperatures, the approaches have, to the best of our knowledge, not been validated for use in complex multicomponent, multiphase mixtures, and at conditions closer to water criticality.

For many applications, phase equilibrium calculations are required in specifications other than pressure and temperature (Nichita, 2024). Thermal simulation models based on a PT-formulation may encounter problems for narrow boiling mixtures, when the conserved energy can fluctuate dramatically with any small change in the primary variable temperature. Using energy as a primary variable in an isenthalpic (PH) or isentropic (PS) flash is therefore preferred (Paterson et al., 2019; Moncorgé et al., 2022; Nichita, 2024; Castier et al., 2015).

We demonstrate that the use of the hybrid-EoS approach is consistent and accurate for the evaluation of thermal properties, thus validating the extension of the framework for fast and accurate isenthalpic and isentropic flashes. For isenthalpic and isentropic state specifications, however, the constraints for thermodynamic equilibrium of the specified state variables cannot all be eliminated explicitly. Michelsen (1987) introduced the Q-functions, modified objective functions that formally eliminate the constraints with Gibbs energy G as the core function. Agarwal et al. (1991) utilized a nested approach of PT-flashes in an inner loop, after which temperature is updated in the outer loop to maximize the Q-function. For such nested phase equilibrium calculations with complex mixtures involving brines, it is thus desirable that PT-flashes are robust, efficient and accurate. We apply the proposed approach to a set of numerical benchmarks of water–gas mixtures using an energy-based specification, to build a case for the use of the hybrid-EoS approach in such simulations.

2. Hybrid-EoS approach for thermodynamic equilibrium at PT specification

At thermodynamic equilibrium, the Gibbs free energy of an equilibrium mixture is at a global minimum. The Gibbs free energy is given by:

$$\overline{G} = G/RT = \sum_{k=1}^{n_p} \sum_{i=1}^{n_c} n_{ik} \ln f_{ik}, \tag{1}$$

with n_{ik} the number of moles of species i in phase k. At the global minimum, the change in Gibbs energy for any transfer of material must be zero:

$$\frac{\partial \overline{G}}{\partial n_{ik}} = \ln f_{ik} - \ln f_{iR} = 0, \quad i = 1, \ldots, n_c; k = 1, \ldots, n_p; k \neq R, \tag{2}$$

where the reference phase R can be any phase. Hence, this yields the equality of fugacity of each component i throughout all phases k as a necessary condition for equilibrium.

2.1. Stability test and phase split

Since it is generally not known in advance how many phases coexist at a global minimum, a sequence of phase stability and split routines must commonly be performed to find the correct equilibrium state.

A stability test indicates whether the Gibbs energy surface is either at or above the mixture tangent hyperplane throughout the entire compositional space (Baker et al., 1982; Iranshahr et al., 2012). Michelsen (1982a) developed a mathematical implementation of this "tangent plane distance" (TPD) criterion. The common approach to finding the minima of the TPD function is to apply local optimization over a set of initial guesses. The corresponding phase compositions can be used as an initial estimate in further phase-split calculations.

In the phase-split procedure, the dimensionless Gibbs energy (1) is minimized with respect to mole numbers. In addition, in SSI iterations or when lnK is used as an independent variable in the Newton method, the material balance must be satisfied:

$$\sum_{j=0}^{n_p-1} \theta_j x_{ij} = z_i, \quad i = 1, \dots, n_c, \tag{3}$$

$$\sum_{i=1}^{n_c} (x_{ij} - x_{i0}) = 0, \quad j = 1, \dots, n_p - 1. \tag{4}$$

Generally, this can be done by introducing equilibrium factors $K_{ij} = \varphi_{ij}/\varphi_{i0}$ and solving the Rachford–Rice (RR) system of equations:

$$R_k \equiv \sum_{i=1}^{n_c} (x_{ik} - x_{i0}) = \sum_{i=1}^{n_c} \frac{z_i(K_{ik} - 1)}{1 + \sum_{p=1}^{n_p-1} \theta_p (K_{ip} - 1)} = 0, \quad k = 1, \dots, n_p; k \neq R. \tag{5}$$

The solution of the RR equations yields the phase fractions $\boldsymbol{\theta} = (\theta_0, \dots, \theta_{n_p-1})^T$ and phase compositions $\mathbf{x}_k$. For two phases, the RR equation can be solved using convex transformations, as proposed by Nichita and Leibovici (2013), leading to a significant increase in solution speed. For multiphase systems, Michelsen (1994) proposed a minimization approach, which was later extended to negative flashes (Leibovici and Nichita, 2008; Yan and Stenby, 2012).

The stability test and phase-split problems have similar mathematical structures. In this work, we adapt the procedures described by Petitfrere and Nichita (2015a,b) for hybrid models. In addition, we have described a fully analytical framework for calculating partial derivatives of the flash and secondary equilibrium properties in Appendix B.

2.2. Description of thermodynamic models

In this work, we use a cubic equation of state (Peng and Robinson, 1976) for the non-aqueous phases and a separate fugacity-activity model for the aqueous phase. In its most basic form, the cubic equation of state is an expression of $P(V, T, \mathbf{n})$. For such models, all residual thermodynamic properties can be derived from their residual Helmholtz free energy form $A^r(V, T, \mathbf{n})$ (Michelsen and Mollerup, 1986; Mollerup and Michelsen, 1992). The pure component properties and binary interaction coefficients for the components considered in the examples in this work can be found in Table 1.

The fugacity-activity model for the aqueous phase involves different expressions for water and dissolved components. For the fugacity of the solvent, water, we follow the description of Jager et al. (2003). They derive the deviation of the chemical potential of H_2O from the pure water state, including the contributions of all molecular and ionic species to water activity:

$$f_w^a = f_{wo} \exp\left[\frac{\mu_w - g_{wo}}{RT}\right]. \tag{6}$$

Table 1
Pure component properties and binary interaction coefficients for cubic EoS.

i	$P_{c,i}$ [bar]	$T_{c,i}$ [K]	ω_i [–]	$k_{i\mathrm{H_2O}}$	$k_{i\mathrm{CO_2}}$	$k_{i\mathrm{CH_4}}$	$k_{i\mathrm{H_2S}}$	$k_{i\mathrm{nC_5}}$
H_2O	220.50	647.14	0.328		0.19014	0.47893	0.105	0.526
CO_2	73.75	304.10	0.239	0.19014		0.0936	0.1093	
CH_4	46.04	190.58	0.012	0.47893	0.0936		0.0912	
H_2S	89.63	373.53	0.0942	0.105	0.1093	0.0912		
nC_5	33.701	469.7	0.2515	0.526				

Here, f_{wo} is the fugacity of an ideal gas at the reference pressure of 1 bar, which is equal to 1. The deviation from ideality follows from the difference between chemical potential μ_w and the Gibbs energy of water in the ideal gas state g_{wo}. The chemical potential μ_w is related to the pure water state with the addition of an activity coefficient $\ln a_w(P, T, \mathbf{x})$, which accounts for the effect of dissolved species, as

$$\frac{\mu_w}{RT} = \frac{g_{w_0,pure}}{RT_0} - \int_{T_0}^{T} \frac{h_{w,pure}}{RT^2}\, dT + \int_{P_0}^{P} \frac{v_{w,pure}}{RT}\, dP + \ln a_w. \tag{7}$$

Here, $g_{w_0,pure}$, $h_{w,pure}$ and $v_{w,pure}$ are the Gibbs energy at reference conditions (T_0, P_0), and enthalpy and molar volume of pure water, respectively.

For the dissolved species, the fugacity has been written in terms of Henry's constants. Models based on Henry's constants are asymmetric activity coefficient models, which means that infinite dilution of the solute is taken as the reference state for the activity coefficient: $h_i^\infty \equiv f_i(P, T)\gamma_i^\infty(P, T, n_k)$. The fugacity of component i in terms of the asymmetric activity coefficient $\tilde{\gamma}_i$ is:

$$f_i(P, T, \mathbf{n}) = h_i^\infty(P, T, n_k)\tilde{\gamma}_i(P, T, \mathbf{n})x_i, \tag{8}$$

where $\tilde{\gamma}_i(P, T, \mathbf{n}) \equiv \gamma_i(P, T, \mathbf{n})/\gamma_i^\infty(P, T, n_k)$.

In our thermodynamic model, Henry's constants are calculated from the approach of Ziabakhsh-Ganji and Kooi (2012). Their model combines Henry's constants for nonelectrolyte solutes following Akinfiev and Diamond (2003). In addition, they included an additional term to account for the effect of brine salinity on gas solubilities, which was first proposed by Duan et al. (1992) and is based on excess Gibbs energies in electrolyte solutions (Pitzer, 1973). Thus, the interaction between dissolved components in the aqueous phase is effectively neglected and $\tilde{\gamma}_i(P, T, \mathbf{n})$ is only dependent on brine salinity. Note that it is possible to use these sets of correlations to include other species as well, but that is not in scope for this work.

2.3. Strategies for phase equilibrium problems at PT

In general, one does not know in advance how many phases coexist at thermodynamic equilibrium, and a sequence of stability testing and phase split procedures has to be performed to find the equilibrium phases. If it is known how many phases can coexist and good initial guesses are available, a negative flash procedure can be used to determine the phase state (Iranshahr et al., 2013a). The domain of the Rachford–Rice equations (5) is bounded by the set of phase fractions θ_k that yield all non-negative phase compositions, which is larger than the physical domain. While the material balance and equifugacity equations may be satisfied in a negative flash, the solution clearly does not yield physically valid phase fractions. More importantly, a negative flash corresponds to a saddle point in the Gibbs energy surface, rather than a minimum (Whitson and Michelsen, 1989).

Nonetheless, the negative flash can be useful for phase-state identification in a multiphase flash. In a two-phase system, θ can take any value between the asymptotes $\theta_{min} = 1/(1 - K_{max})$ and $\theta_{max} = 1/(1 - K_{min})$. In systems that are known to form two phases at maximum, converging to a non-trivial solution with a negative flash indicates the single-phase stability of the feed with the same certainty as a traditional phase stability test (Whitson and Michelsen, 1989).

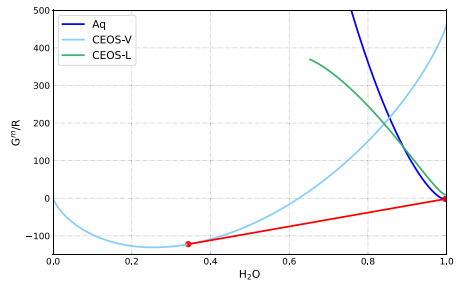

Fig. 1. Gibbs energy of mixing surfaces of H_2O–CO_2 mixture at P = 30 bar and $T = 450$ K. Aq is aqueous phase fugacity model, $CEOS-V$ and $-L$ denote the vapour- and liquid-like real roots (if present) of the cubic EoS. The red line is tangent to the single-phase Gibbs energy surface at the equilibrium phases. Feed compositions between the red dots will split into two phases.

In multiphase systems, however, phase-state identification based on negative flash is not sufficient. If one knows the maximum number of phases, the solution of the flash procedure can only be confirmed for all positive phase fractions, i.e., it cannot confirm the phase state of a single- or two-phase mixture with a three-phase negative flash. Additional two-phase negative flash computations would be required to identify the equilibrium state, because the phase behaviour outside the three-phase region may be different from the results of the negative flash (Leibovici and Neoschil, 1995; Iranshahr et al., 2010). Complemented with the parametrization technique, the negative flash approach can still be used for robust evaluation of complex multiphase systems (Iranshahr et al., 2013b).

For some applications of interest, such as subsurface gas production and storage, sequestration of supercritical CO_2 in saline aquifers and geothermal energy production, the assumption of a maximum of two phases is reasonable. In these cases, a two-phase negative flash approach initialized with K-values based on Henry's constants may be the preferred choice. This approach is limited to liquid water conditions and cannot handle the transition from liquid water to steam. In addition, this simplification is not valid in more complex multiphase systems, and a full Gibbs energy minimization procedure is required.

2.4. Practical challenges for hybrid-EoS approach

The hybrid-EoS approach is best illustrated by a graphical representation of the different equations of state. The Gibbs free energy surfaces describe the hypothetical single-phase conditions throughout the compositional space. For a given feed composition **z**, the global equilibrium state corresponds to a linear combination of the compositions of the coexisting equilibrium phases, located on the tangent hyperplane to the Gibbs free energy surface (or, equivalently, Gibbs free energy of mixing). The hyperplane is below or equal to the Gibbs energy surfaces at all compositions.

In Fig. 1, the Gibbs free energy of mixing surfaces for a binary system H_2O–CO_2 at given pressure and temperature of the vapour(-like) root, liquid(-like) root and aqueous fugacity model are shown. The cubic EoS is valid for all compositions, but the fugacity model for the aqueous phase is limited to H_2O-rich compositions.

2.4.1. Root selection

From Fig. 1, it can be observed that at H_2O-rich compositions, there can be a minimum of both the liquid(-like) root of the cubic EoS and aqueous fugacity model. Nonetheless, they both describe the liquid water phase. We thus need to identify the root types of the cubic EoS, ignore any water-rich liquid(-like) root and select the vapour-like root instead.

The cubic EoS is generally expressed in terms of the compressibility factor Z to solve for density at specified pressure and temperature. The cubic polynomial has three roots, of which either one or three are real. It is only inside the mechanical spinodal that three real roots can be obtained, the spinodal denoting the limits of mechanical stability ($\partial P/\partial V < 0$) which coincide at the mechanical critical point (Imre and Kraska, 2005). In the case of three real roots, the smallest volume corresponds to the liquid phase and the largest root represents the vapour phase. For pressures below the mechanical spinodal, the single real root is associated with the vapour phase, whereas at higher pressures the phase is a liquid. We can identify these roots using the characteristics of the cubic polynomial (Kamath et al., 2010).

2.4.2. Stability test and phase split

Contrary to the equation of state, the fugacity model for the aqueous phase has been developed only to describe a water-rich liquid phase. Furthermore, the Gibbs energy surface in this model is convex throughout the relevant range of compositions. We therefore have only a single local minimum of the Gibbs energy, which allows us to use a specific initial guess.

In addition, for problems where the fugacity coefficients are only weakly dependent on the phase composition, the SSI procedures for stability testing and phase split converge rapidly (Michelsen, 1982b). In fact, the use of a Newton procedure may not even improve performance, as the computational cost of evaluating derivatives and solving the linear system is relatively large. In addition, it is important for both stability test and phase split updates to check if the composition remains within the specified range to prevent unphysical updates of aqueous properties.

2.4.3. Range of validity

A thermodynamically consistent equation of state is capable of describing the continuity of fluid between gas and liquid phase states beyond the critical point. When choosing different thermodynamic models for aqueous and other fluid phases, however, there is no such continuous transition, and no critical point exists. Therefore, it is not possible to identify the criticality of water-rich phases, and the accuracy of the hybrid-EoS approach decreases in the vicinity of solvent criticality and beyond.

The models considered in this study have been extensively validated with experimental data for binary systems of water or brines with a single solute at moderate temperatures (Ziabakhsh-Ganji and Kooi, 2012; Duan et al., 1992). To assess the range of applicability for the proposed approach, we attempt to reproduce experimental values of Tödheide and Franck (1963). They measured phase equilibria of the H_2O–CO_2 system at near-critical conditions for the solvent. Although our approach is unable to describe the critical curve, Fig. 2 shows that the hybrid-model approach is reproducing experimental results accurately up to conditions relatively close to solvent criticality. The data points represent measured dew point and bubble point curves. For Fig. 2a, the Root Mean Square Error (RMSE) for all experimental points is 1.6%, while for Fig. 2b, RMSE = 2.2%.

The accuracy of the method is inherently a result of its parametrization. However, the results of the same binary system but modelled with an association model (CPA EoS Kontogeorgis et al., 1996, Fig. 3), indicate that more advanced models do not necessarily improve the predictions. Here, for Fig. 3a, the RMSE = 2.6%, while for Fig. 3b, the RMSE = 5.9%. Critical conditions are not a problem here, but the improved description of the aqueous phase is at the expense of a worse prediction of the non-aqueous phase. Besides, the intended improvement in accuracy of association models comes with the computational cost of an iterative density solver, which presents an obvious advantage of the proposed hybrid-EoS approach.

Notice that at temperatures too close to the critical temperature, the proposed algorithm becomes unpredictable. This is because the logic for root selection relies on the characteristics of the cubic polynomial, which is only valid below the temperature at which a mechanical spinodal exists (Section 2.4.1). At temperatures above, this approach

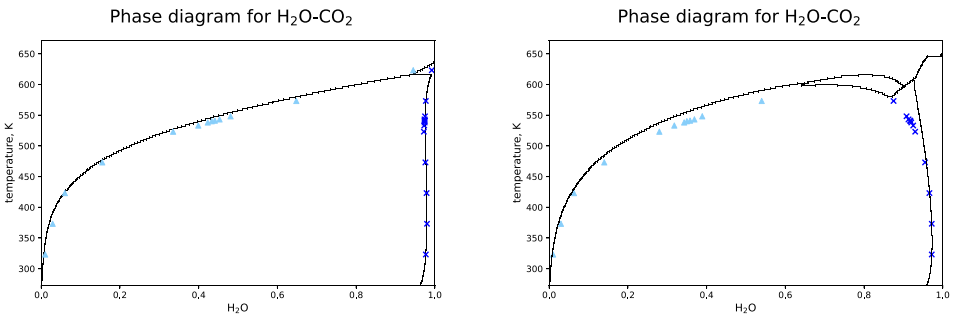

(a) P = 200 bar (b) P = 500 bar

Fig. 2. Hybrid-EoS temperature-composition diagrams for H_2O–CO_2 mixture at different pressures. CO_2-rich phase composition is indicated by ▲, aqueous composition by ×.
Source: Solubility data from Tödheide and Franck (1963).

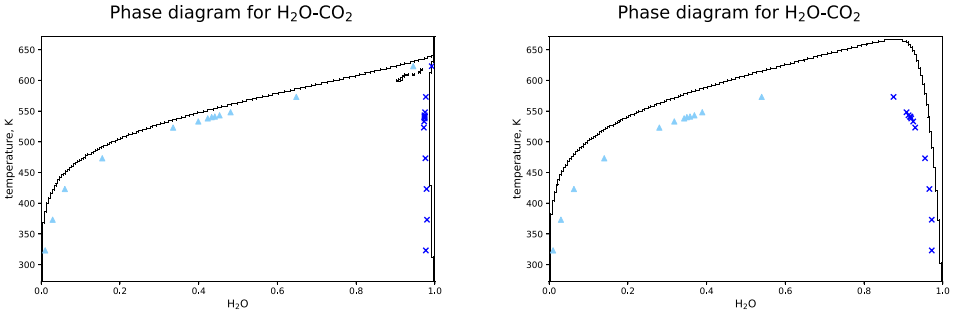

(a) P = 200 bar (b) P = 500 bar

Fig. 3. CPA EoS temperature-composition diagrams for H_2O–CO_2 mixture at different pressures. CO_2-rich phase composition is indicated by ▲, aqueous composition by ×.
Source: Solubility data from Tödheide and Franck (1963).

is no longer adequate. In Fig. 4, the ranges of validity for the proposed hybrid-EoS approach are investigated with regard to binary H_2O–CO_2 mixtures at conditions approaching brine criticality. The solid line indicates the maximum temperature for the hybrid-EoS approach, according to the mechanical spinodal. The actual critical line for the H_2O–CO_2 system (indicated by ⋆) is located slightly above. Below this upper limit, it can be observed that the accuracy of the aqueous model decreases at elevated temperatures and pressures. This is due to the increased solubility of the solute, which increasingly violates the assumption in Henry's coefficient models that interaction between solutes is negligible. In addition, the aqueous model is not developed to model the behaviour of the solvent at conditions close to criticality.

It must be noted that the H_2O–CO_2 system under high-pressure conditions depicted in Figs. 2 and 3 tends to form hydrates in low temperature regions. The framework can be easily extended to include a hydrate EoS, adding another Gibbs energy surface to Fig. 1, but that is beyond the scope of this work.

2.5. Results of PT-flash calculations

We apply the hybrid-EoS framework to gas mixtures of interest. The models considered in this study have been extensively validated with experimental data for binary systems of water or brines with a single solute at moderate temperatures and we have established a range of applicability in the previous section. Unfortunately, a limited number of experimental measurements have been reported to validate the solubility of different gas mixtures that fit the scope of modelling subsurface energy transition applications. Apart from H_2O, the components that exist in most notable quantities in such applications are generally CO_2, CH_4 and (traces of) light hydrocarbon fractions, H_2S and salt/ions. With increasingly low solubility, the effect of heavier hydrocarbons on the aqueous phase and other solutes becomes negligible and the relative importance of the interaction between H_2O and such components decreases. Dhima et al. (1999) and Qin et al. (2008) reported a small set of solubility data of the H_2O–CH_4–CO_2 ternary system. Huang et al. (1985) performed a thorough investigation of the equilibrium compositions and phase boundaries in two gas mixtures of CH_4–CO_2–H_2S in contact with water. One of the mixtures was rich in CO_2 and the other in H_2S, resulting in the appearance of a three-phase region with a dense CO_2 and H_2S rich phase, respectively. The effect of brine salinity on the solubility of CO_2–H_2S mixtures was studied by Savary et al. (2012).

2.5.1. H_2O–CH_4–CO_2 mixture

Qin et al. (2008) measured vapour–liquid equilibria of the H_2O–CH_4–CO_2 ternary system at temperatures of 324 K and 375 K and pressures from 100 to 500 bar. They reported data on the solubility of pure gases and mixtures of CH_4 and CO_2. Fig. 5 displays the results of the hybrid-EoS approach for gas solubility at 375 K and a range of pressures. Under these conditions, the non-aqueous phase does not split into multiple phases or undergo a phase transition, it merely varies between vapour-like and liquid-like. The ternary diagrams show only the water-rich end of compositions, from 97% to 100% H_2O. The dots indicate the solubilities, and the tie-lines represent feed compositions for which the same equilibrium phases will be obtained.

2.5.2. H_2O–CH_4–CO_2–H_2S mixture

Huang et al. (1985) reported solubility data and phase boundaries of two CH_4–CO_2–H_2S mixtures with water over a wide range of temperatures and pressures. Here, two cases are considered with CO_2 and

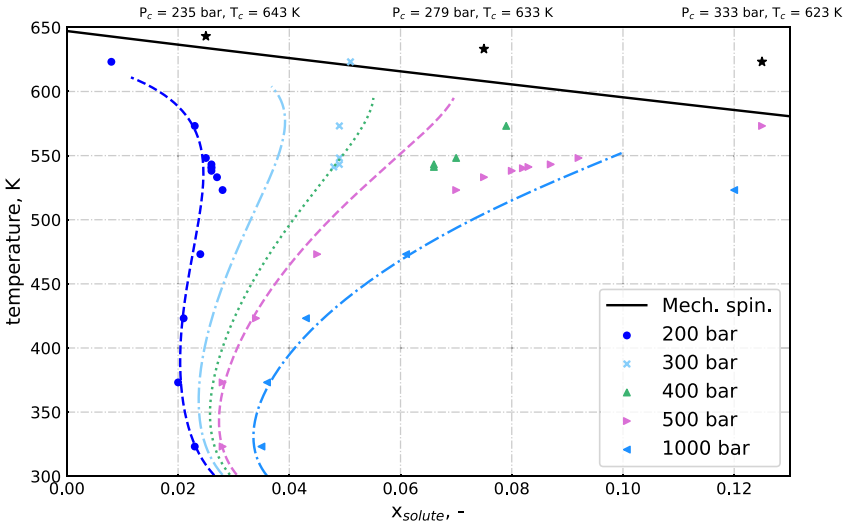

Fig. 4. Illustration of validity of proposed hybrid-EoS approach for binary mixture H_2O–CO_2. Solid line represents upper limit of temperature where pressure equation for cubic EoS exhibits mechanical spinodal. This is the maximum temperature where one can identify cubic root as V/L by means of cubic polynomial. The hybrid-EoS approach becomes unstable near this upper bound. Points along the critical line with respect to composition are indicated by ⋆. Curves indicate CO_2 solubilities in H_2O for a range of pressures.
Source: Solubility and critical point data from Tödheide and Franck (1963).

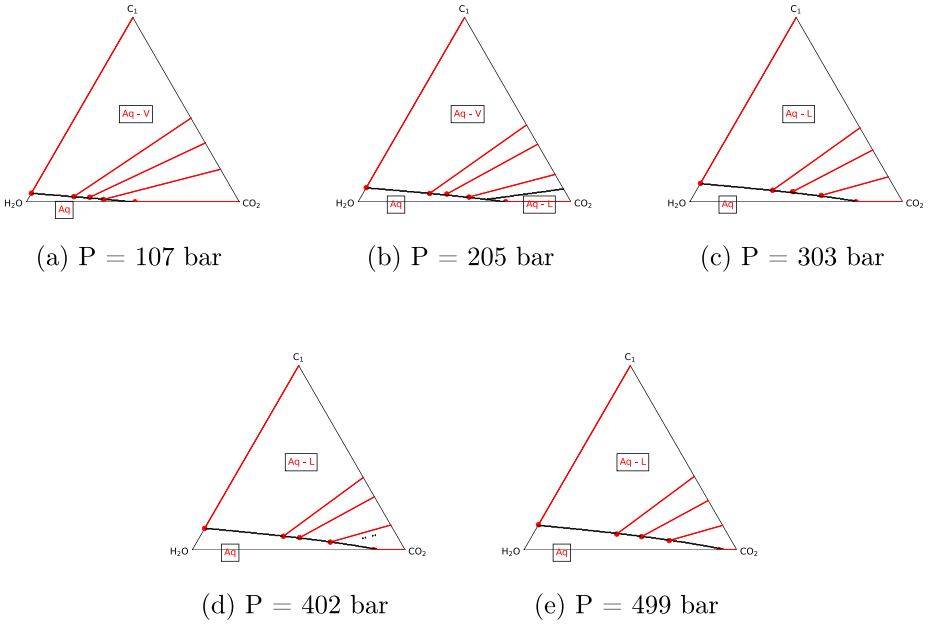

Fig. 5. Ternary diagram for H_2O–CH_4–CO_2 mixtures at 375.6 K, zoomed in to 97%–100% H_2O. Black lines are phase boundaries, red lines are tie-lines that connect the solubility endpoints.
Source: Solubility data from Qin et al. (2008).

H_2S rich mixtures. The PT-diagrams of the mixtures (Fig. 6) show the single-, two- and three-phase regions with Aq, V and L phases. At low temperatures, the system exhibits three-phase behaviour with a dense CO_2-phase (a) or a dense H_2S-rich phase (b). Note that the change from vapour-like to liquid-like phases beyond the three-phase envelope is not a physical phase change, but originates from phase labelling.

Fig. 7 shows the solubility curves of the two mixtures along the isotherms indicated in Fig. 6. The solubility of gases heavily depends on gas composition. The y-axes for each of the components are equal between mixtures 1 and 2, but the variation in gas composition creates a difference in solubility of up to an order of magnitude. This effect may play a significant role in the dynamics of subsurface applications. While the proposed hybrid EoS qualitatively predicts this behaviour, the overall deviation of the predicted solubilities against experimental results is relatively high with RMSE = 12.8%.

Furthermore, note that the slope of the solubility curves are discontinuous across phase boundaries. This occurs along the isotherms of 37.8 °C (311 K) and 65.6 °C (339 K) for mixture 2, where the three-phase region with the H_2S-rich liquid is crossed. At the pressures associated with the three-phase boundary, the slope of the solubility curve is altered, even though the phase changes do not involve the aqueous phase.

2.5.3. *Brine-CO_2–H_2S mixture*

Savary et al. (2012) studied the solubility of CO_2–H_2S mixtures in pure water and 2 molal NaCl solution (moles of solute per kg of pure

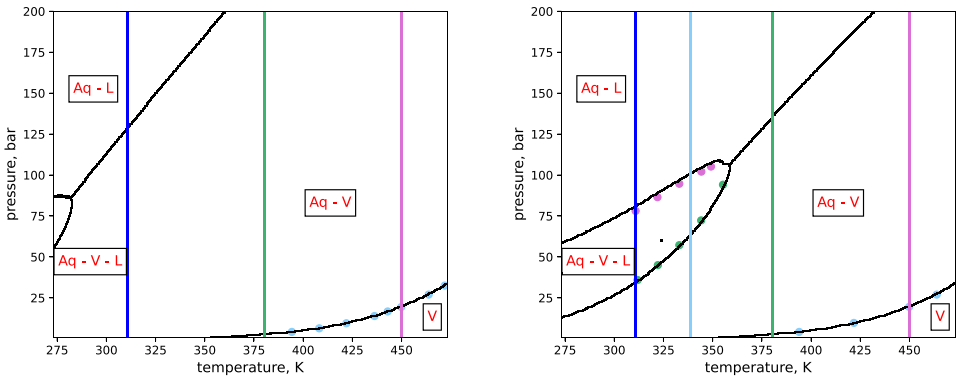

(a) Mixture 1: 0.50/0.15/0.30/0.05 (b) Mixture 2: 0.50/0.05/0.05/0.40

Fig. 6. PT diagram for H_2O–CH_4–CO_2–H_2S mixtures. Dew point (V/Aq, blue) and three-phase boundary data (L/L_{H_2S}, pink, and V/L_{H_2S}, green) from Huang et al. (1985). Solubility curves along isotherms are shown in Fig. 7.

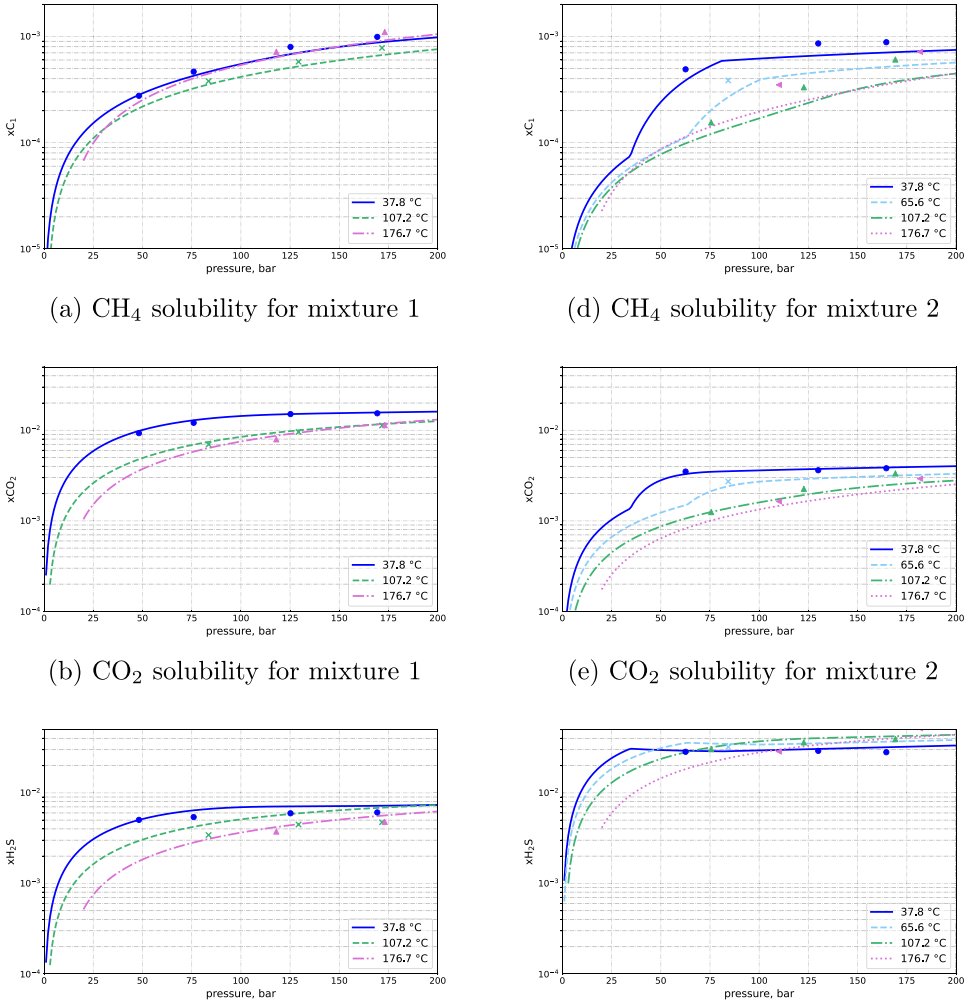

(a) CH_4 solubility for mixture 1 (d) CH_4 solubility for mixture 2

(b) CO_2 solubility for mixture 1 (e) CO_2 solubility for mixture 2

(c) H_2S solubility for mixture 1 (f) H_2S solubility for mixture 2

Fig. 7. Solubility of solutes in aqueous phase for H_2O–CH_4–CO_2–H_2S mixtures: (a,b,c) 0.50/0.15/0.30/0.05, (d,e,f) 0.50/0.05/0.05/0.40. *Source:* Solubility data from Huang et al. (1985).

solvent, denoted M) at a temperature of 393.15 K. The results of the hybrid-EoS approach for gas solubility in 0M and 2M brines of gas mixtures with different compositions, indicated by the ratios, are shown in Fig. 8. Under these high-temperature conditions, no three-phase conditions occur. As expected, the order of solubility curves of CO_2 and H_2S between gas composition ratios is reversed. The experimental study reported difficulties with measurements of ternary mixtures at high pressures, leading to uncertainties, in part due to the toxicity of H_2S. Nonetheless, the data clearly show a salting-out effect of the gases as a result of brine salinity, a phenomenon that can be captured

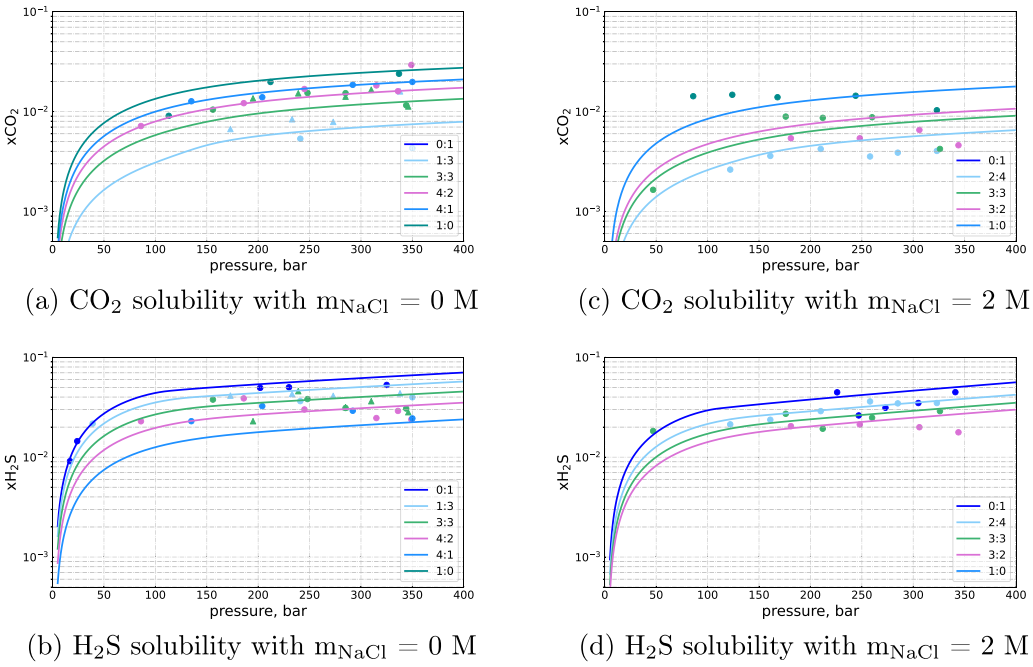

(a) CO_2 solubility with $m_{NaCl} = 0$ M (c) CO_2 solubility with $m_{NaCl} = 2$ M

(b) H_2S solubility with $m_{NaCl} = 0$ M (d) H_2S solubility with $m_{NaCl} = 2$ M

Fig. 8. Solubility of CO_2 and H_2S in aqueous phase for H_2O–NaCl–CO_2–H_2S mixtures with different NaCl molalities [mol/kg] at T = 393.15 K. Ratios indicate mole fraction ratios of CO_2 to H_2S in the feed.
Source: Solubility data from Savary et al. (2012).

reasonably well with our modelling approach. Here, overall RMSE against experimental solubilities is 8.5%.

3. Hybrid-EoS approach for thermodynamic equilibrium at *PH* and *PS* specifications

In many cases, enthalpy or entropy is a better choice than temperature for use as a nonlinear unknown in reservoir simulation (Moncorgé et al., 2022). This requires thermodynamic equilibrium to be performed at isenthalpic or isentropic conditions. While a PT-flash can be performed as an unconstrained minimization, the constraints of specified state variables cannot all be eliminated explicitly in the case of an isenthalpic or isentropic state specification (Michelsen, 1987, 1999). In a PH-flash, the minimization formulation reads:

$$\min\ (-S)(P^{spec}, T, \mathbf{z}), \tag{9a}$$

s. t.

$$H(P^{spec}, T, \mathbf{z}) - H^{spec} = 0. \tag{9b}$$

For a PS-flash:

$$\min\ H(P^{spec}, T, \mathbf{z}), \tag{10a}$$

s. t.

$$S(P^{spec}, T, \mathbf{z}) - S^{spec} = 0. \tag{10b}$$

Such constrained minimization procedures can be formulated based on a single 'Q-function' (Michelsen, 1987, 1999). For an isenthalpic flash,

$$Q^H(P, T, \mathbf{z}) = \frac{G(P, T, \mathbf{z}) - H^{spec}}{T}. \tag{11a}$$

By fixing the pressure P and composition $\mathbf{z}$, $Q^H = Q^H(T)$ becomes a function that can be optimized for temperature. The gradient vector and its derivative then read

$$g^H(T) = \frac{\partial Q^H}{\partial T} = -\frac{1}{T^2}(H - H^{spec}), \tag{11b}$$

$$g^{H'}(T) = \frac{\partial^2 Q^H}{\partial T^2} = \frac{2}{T^3}(H - H^{spec}) - \frac{1}{T^2}\left(\frac{\partial H}{\partial T}\right)_{P,\mathbf{z}}. \tag{11c}$$

Note that the gradient of Q^H with respect to temperature essentially reduces to the enthalpy specification equation. Similarly, for the isentropic specification:

$$Q^S(P, T, \mathbf{z}) = G(P, T, \mathbf{z}) + TS^{spec}, \tag{12a}$$

with the gradient vector and its derivative

$$g^S(T) = \frac{\partial Q^S}{\partial T} = \left(\frac{\partial G}{\partial T}\right)_{P,\mathbf{z}} + S^{spec} = -S + S^{spec}, \tag{12b}$$

$$g^{S'}(T) = \frac{\partial^2 Q^S}{\partial T^2} = -\left(\frac{\partial S}{\partial T}\right)_{P,\mathbf{z}}. \tag{12c}$$

The calculation of thermodynamic properties G, H and S will be described in Appendix A. Evaluation of $g'(T)$ of the specific Q-function with respect to temperature requires derivatives of the PT-flash procedure (see Appendix B).

It is possible to optimize the Q-function using second-order methods. Alternatively, the maximum of Q can be obtained using a nested approach of standalone PT-flashes to calculate Q, $g(T)$ and $g'(T)$ and to locate the zero gradient $g(T)$ using a root-finding method (Agarwal et al., 1991; Xu et al., 2025).

The hybrid EoS approach is an interesting candidate for nested PH- and PS-flashes of mixtures with brine. Firstly, the thermodynamic models considered in this work are evaluated at P, T, and composition at low computational cost during PT-flash calls, while maintaining their accuracy for phase equilibrium calculations. In addition, we demonstrate that the use of the models considered in our approach is consistent and accurate for evaluation of thermal properties, thus validating the extension of the hybrid-EoS approach to any P-based state specification.

3.1. Root-finding methods for solving the state specification equation

The outer loop of the nested algorithm consists of solving the temperature for which the state specification equation is satisfied.

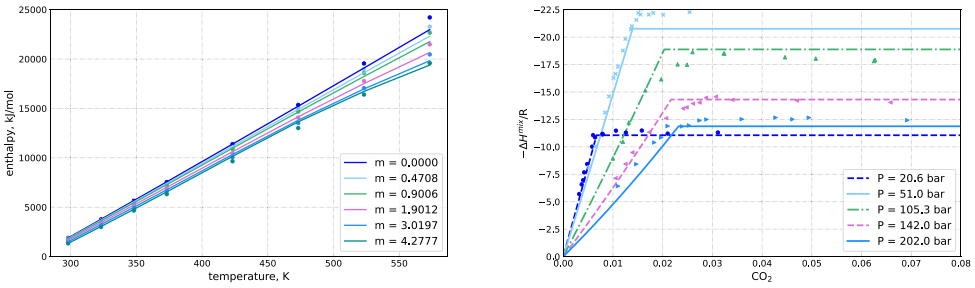

(a) Water/brine enthalpy at saturation pressure

(b) Enthalpy of dissolution at T = 323.15 K

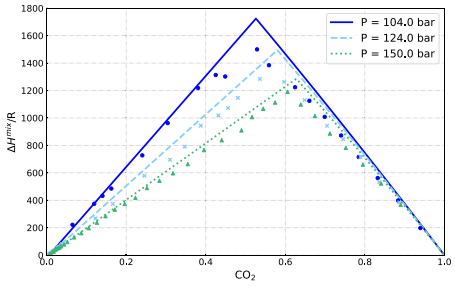

(c) Enthalpy of mixing at T = 523.15 K

Fig. 9. Water/brine enthalpy at various NaCl molalities m [mol/kg] and enthalpies of dissolution and mixing for CO_2–H_2O systems. Data from Pitzer et al. (1984) (a), Koschel et al. (2006) (b) and Chen et al. (1992) (c).

By definition, the enthalpy or entropy increases monotonically with temperature. In case of a phase transition, $H(T)$ or $S(T)$ may exhibit a sharp nonlinearity that is difficult to capture in the PT-domain. However, consistent bracketing of the lower and upper temperature bounds for the solution, combined with a robust PT flash in the inner loop, guarantees the location zero of (11b) or (12b), even in the limiting case of a discontinuity at a singular transition temperature T^* in the objective function (Moncorgé et al., 2022). These conditions occur when an n_c-component mixture encounters an $(n_c + 1)$-phase state. Gibbs phase rule dictates that at such phase boundary, only one degree of freedom is left and temperature or pressure becomes a dependent variable. A PT-flash may find either of two states a and b with equal Gibbs free energies (Sun et al., 2017):

$$G^a(P, T^*, \mathbf{z}) = G^b(P, T^*, \mathbf{z}). \tag{13}$$

Along an isobar (or isotherm), the total enthalpy or entropy of the system exhibits a discontinuity due to the transition from state a to state b. The temperature (or pressure) of the system is invariant and can only change when the energy variable has sufficiently increased or decreased. The phase state that does satisfy the specified state X^{spec} is described by a linear combination of two PT-flashes at values X^a and X^b with weights β and $(1 - \beta)$:

$$X^{spec} = \beta X^a + (1 - \beta) X^b, \tag{14a}$$

where

$$\beta = \frac{X^{spec} - X^b}{X^a - X^b}. \tag{14b}$$

In this work, we follow the procedure for nested isenthalpic flashes by Xu et al. (2025), using a hybrid approach of derivative-free Brent (Brent, 1971), and Newton methods. A lower and upper bound for temperature, and possibly a good initial guess from a previous flash, are determined to initiate Brent's method iterations. These will converge rapidly in most cases that do not involve a transition temperature or are close to a critical point. Note that with the hybrid-EoS approach, the bounds should remain within the temperature range of applicability, that is, below critical conditions (Section 2.4.3), and if no ice or hydrate phase is considered, above the freezing point of water.

Under difficult conditions, both the inner loop of PT-flashes, as well as the outer loop of temperature updates, may take many iterations to converge and therefore a gradient-based update of temperature can improve performance. To do this, Newton steps can be safely performed to improve convergence if the curvature of the objective function allows. The convergence criterion for a Newton step is given by

$$g(T) \cdot g''(T) > 0, \tag{15}$$

where the second derivative of the objective function $g''(T)$ is approximated using numerical derivatives.

In addition, Xu et al. (2025) suggested an extrapolation method to estimate compositions for PT-flash initialization after a temperature update, using the partial derivatives of the previous PT-flash with respect to temperature:

$$\mathbf{n}_{est} \approx \mathbf{n} + \frac{\partial \mathbf{n}}{\partial T} s_{try}. \tag{16}$$

The value of s_{try} should be determined iteratively. We have extended the development of fully analytical partial derivatives for isenthalpic and isentropic flashes, including those at transition temperatures, in Appendix B.

3.2. Accuracy and consistency of the hybrid-EoS approach for P-based flash calculations

To apply the hybrid-EoS framework to PH and PS state specifications, it is important to assess the accuracy and consistency of thermal properties evaluated from the thermodynamic models (see Appendix A). The enthalpy and entropy should be monotonically increasing with temperature, or equivalently, heat capacity must be positive at all conditions:

$$\left(\frac{\partial H_j}{\partial T}\right)_{P,\mathbf{n}} = C_{Pj} > 0 \tag{17}$$

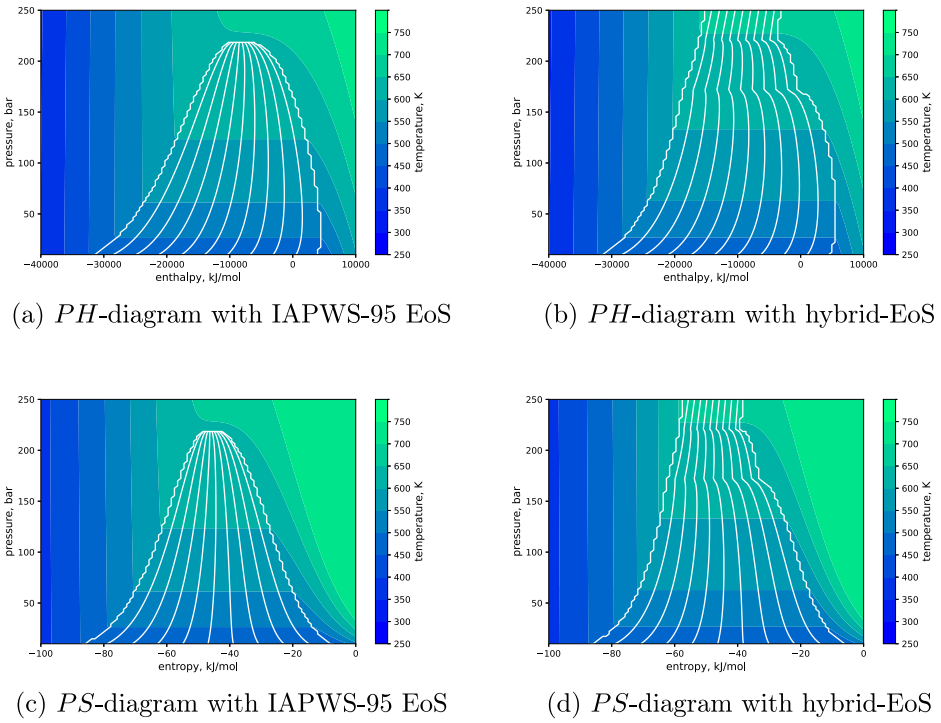

(a) PH-diagram with IAPWS-95 EoS (b) PH-diagram with hybrid-EoS

(c) PS-diagram with IAPWS-95 EoS (d) PS-diagram with hybrid-EoS

Fig. 10. Comparison of pure H_2O PH- and PS-diagrams from hybrid-EoS approach with IAPWS-95 EoS (Wagner and Pruß, 2002). As expected, the isotherms in the two-phase region start to deviate and eventually become inconsistent close to the critical point.

Fig. 9 compares aqueous phase enthalpies and enthalpies of mixing with experimental data. The enthalpy of pure H_2O and H_2O–NaCl brines at saturation pressures has been measured by Pitzer et al. (1984), shown in Fig. 9a. Molar heat capacities are positive, slightly lowered by the presence of ions and slightly deviate at higher temperatures. Enthalpies of CO_2 dissolution into the aqueous phase were reported by Koschel et al. (2006), shown here for a temperature of 323.15 K in Fig. 9b. The y-axis has been inverted; a negative enthalpy of mixing for CO_2 dissolution indicates the exothermic nature of the process. The enthalpy of mixing reaches a plateau at the solubility limit of CO_2 into H_2O at the specific pressure and temperature, and any additional CO_2 does not dissolve into the aqueous phase. Total enthalpies of mixing across the entire composition range have been measured by Chen et al. (1992), Fig. 9c. The distinct linear shapes of these curves, compared to smooth enthalpies of mixing for gas mixtures, result from the two-phase behaviour of this system. The corresponding overall RMSE for all 3 types of enthalpies are 5.6%, 1.2% and 3.3% respectively.

3.3. Results of PH- and PS-flash calculations

We extend the application of the hybrid-EoS framework to PH- and PS-flashes. It is not straightforward to validate isenthalpic and isentropic phase equilibria with experimental data, and, as a result, not many experimental benchmarks are available. We compare the results of two-phase envelopes in PH- and PS-domains for pure H_2O with those obtained from the IAPWS-95 reference EoS for water and steam (Wagner and Pruß, 2002). In addition, we reproduce the numerical benchmark of the H_2O–nC_5 (pentane) mixture (Agarwal et al., 1991; Di Zhu and Okuno, 2015) and investigate its behaviour throughout the compositional domain. Finally, we explore the nature of isenthalpic phase equilibria to a ternary mixture of H_2O–CH_4–CO_2, which is pivotal for modern energy transition applications.

3.3.1. H_2O phase envelopes

Fig. 10 shows the two-phase envelopes where liquid water and steam coexist in the PH- and PS-space, as modelled with the IAPWS-95 reference EoS for pure water and steam (Wagner and Pruß, 2002). At enthalpies below and above the two-phase region, the system is in a single-phase liquid water and steam state, respectively. Using a consistent equation of state such as IAPWS-95, the saturation curves coincide at the critical point, which for H_2O is around 220 bar and 647 K. As stated before, the use of different thermodynamic models for aqueous and vapour phases introduces an inconsistency towards the critical point, and that is mostly evident at temperature above 650 K. However, the accuracy of the temperature contours within the range of interest for many energy transition subsurface applications well below the critical temperature is satisfactory.

3.3.2. H_2O–nC_5 mixture

Agarwal et al. (1991) and Di Zhu and Okuno (2015) investigated isenthalpic flashes of an equimolar mixture of water and pentane along an isobar of 10 bar. The results for this binary mixture using the proposed approach are shown in Fig. 11. From the temperature-composition diagram (Fig. 11a), it is evident that the isobars cross different phase states for different compositions. The nC_5-rich mixture starts from $Aq-L$ conditions, then crosses a small $V-L$ region and then enters the single-phase vapour state. The other compositions cross a region of $Aq-V$, rather than $V-L$. In all cases depicted here, the three-phase boundary of $Aq-V-L$ states is crossed. By definition, such a three-phase transition for a binary system occurs at a single transition temperature T^*.

The phase transitions also appear in the total enthalpies along the isobars (Fig. 11b). Within regions, enthalpies increase smoothly, but at any phase transition, the slopes are discontinuous. At the transition temperature of 387 K, total enthalpy jumps from $Aq-L$ to $V-L/Aq-V$ states, as prescribed by (13).

Fig. 11c shows the phase equilibria for the H_2O–nC_5 mixture under the same conditions, but now in the enthalpy-composition domain. The isobars represent the same temperature ranges, but because reference enthalpies for each component are different, such a diagram is skewed and less straightforward to analyse. Still, the same phase regions can be observed while moving along the enthalpy axis. Contrary to the temperature-composition diagram, however, the three-phase boundary now appears as a region of constant temperature that must be crossed in order for the temperature to change again.

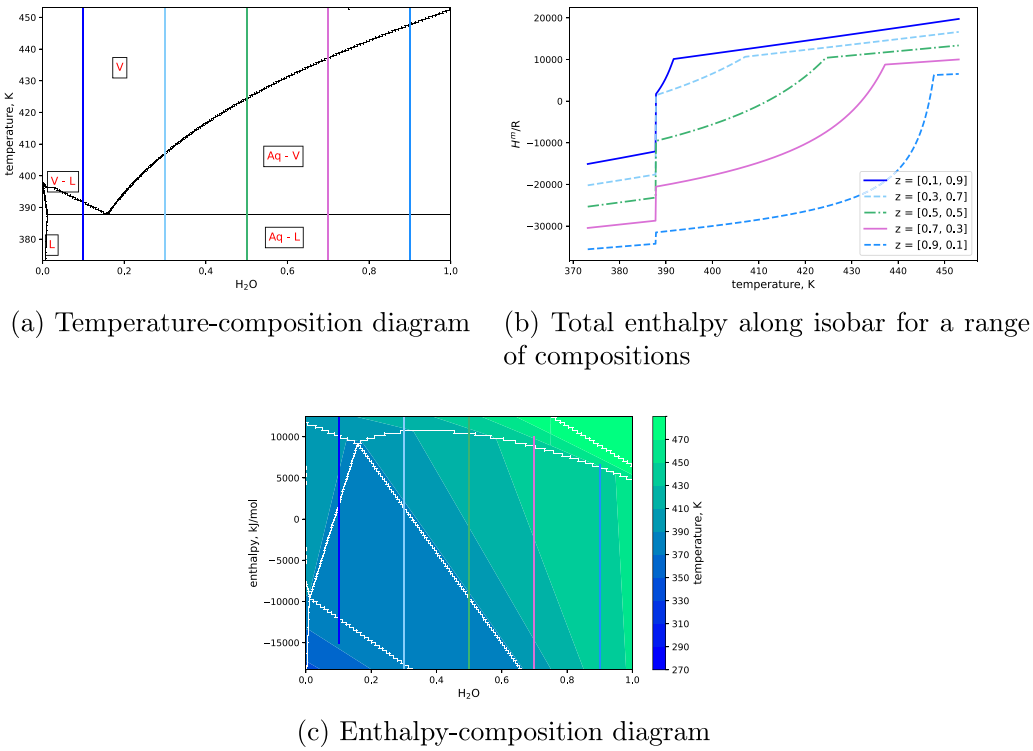

(a) Temperature-composition diagram

(b) Total enthalpy along isobar for a range of compositions

(c) Enthalpy-composition diagram

Fig. 11. Isothermal and isenthalpic flashes for H_2O–nC_5 mixture at 10 bar. A transition temperature occurs at 387 K, where three phases coexist for the binary system. The transition occurs along almost the entire range of compositions. The lines correspond to the isobars for five different compositions in each diagram.

3.3.3. H_2O–CH_4–CO_2 mixture

A simple representation of CO_2 sequestration in depleted gas fields involves a ternary mixture of H_2O–CH_4–CO_2. In such CO_2 injection operations, high-purity CO_2 is injected into a depleted gas reservoir, often at relatively low pressure conditions with large saturations of CH_4 gas. Due to expansion cooling and phase transitions in the wellbore and upon expanding into the low-pressure reservoir, the system may encounter the pressure–temperature ranges depicted in this example. These conditions are particularly important with regard to the appearance of liquid CO_2, which results in complex three-phase dynamics in the simulation.

Fig. 12a–c present ternary diagrams of this mixture at a pressure of 70 bar and three different temperatures (280–290–300 K), close to the critical point of pure CO_2. Under these conditions, which are not unlikely in CO_2 injection processes into depleted gas reservoirs, a three-phase region of $Aq - V - L_{CO_2}$ exists. It is under these circumstances that simulation models which employ a PT-formulation will struggle to converge.

This is, again, illustrated by the shape of the total enthalpies along isobars. Fig. 12d is a quasi-binary temperature-composition diagram with mole fractions of H_2O–CH_4 at a constant ratio — along the blue dotted lines in Fig. 12a–c. This can be thought of as being the original composition of the depleted gas reservoir, into which pure CO_2 is injected. The temperature-composition diagram clearly shows the presence of the three-phase envelope that degenerates at the critical point for pure CO_2. Notice that the blue dotted line crosses the three-phase region at very different feed compositions throughout the increase from 280 to 300 K, which indicates how sensitive this system is to changes in thermodynamic state.

The phase transitions also appear in the total enthalpies along the isobars (Fig. 12e). The curves are shown for different compositions, corresponding to the lines in Fig. 12d. In this ternary mixture, we do not observe phase transitions where an $(n_c + 1)$-state would occur, and thus no transition temperatures exist as such. Yet, the curves show an increasingly nonlinear trend when approaching pure CO_2 conditions, which will reduce to the $V - L$ transition at pure CO_2. These nonlinearities are problematic for PT-based simulation models.

4. Conclusions

This paper presents a framework to combine different thermodynamic models for various phase types in multiphase equilibrium calculations. The hybrid-EoS approach was applied to calculate equilibria of reservoir mixtures with brine by using a cubic EoS for the non-aqueous phase and a separate fugacity-activity model for the aqueous phase. The fugacity-activity model is based on Henry's constants for solutes, an activity coefficient to account for brine salinity and a separate fugacity model for the water component. The computational efficiency of cubic EoSs can be maintained, while aqueous phase properties can be evaluated to good accuracy at low computational cost.

Using different thermodynamic models will yield multiple minima of the Gibbs free energy surfaces in water-rich compositions. It is important to distinguish the vapour and liquid roots of the cubic EoS in water-rich compositions and identify the correct minima in the Gibbs energy surfaces accordingly. Furthermore, the hybrid-EoS approach introduces an inconsistency towards the critical conditions of the brine phase. A range of applicability is established, yielding robust, accurate and efficient solution procedures away from critical conditions. In addition, the computational cost of evaluating stability tests for different phases can be reduced by assigning specific sets of initial guesses. Satisfactory predictions of mutual solubilities of gases and water have been obtained, and we have validated the approach by comparing our phase equilibrium calculations with experimental data of a set of relevant gas mixtures with water.

Furthermore, we have assessed the accuracy and consistency of thermal properties evaluated from the hybrid-EoS approach against a set of experimental data of aqueous phase enthalpies and enthalpies of mixing. This validates the extension of the framework to enthalpy- and entropy-based equilibrium calculations. Such PH- and PS-flashes

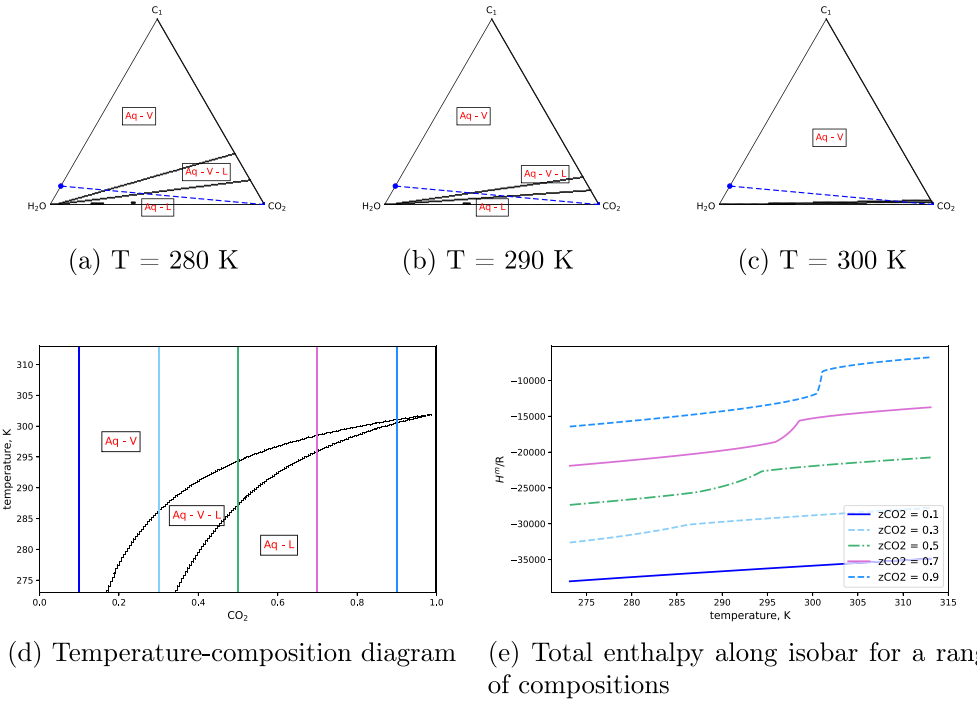

(a) T = 280 K (b) T = 290 K (c) T = 300 K

(d) Temperature-composition diagram (e) Total enthalpy along isobar for a range of compositions

Fig. 12. Isothermal flashes for H_2O–CH_4–CO_2 mixture at 70 bar. The temperature-composition diagram and isobars are evaluated across the pseudo-binary mixture along the dotted line in a/b/c of constant H_2O–CH_4 ratio of 0.9/0.1. No transition temperature can be observed under these conditions, even though the slope of the isobars increases significantly with higher CO_2-content.

are often solved using a nested approach of isothermal flashes with a temperature update in the outer loop. In addition to a robust and efficient inner loop of *PT*-flashes, gradient based methods have been implemented to improve the performance of the outer loop and provide an improved initial guess for the *PT*-flash iteration. We described a fully analytical framework for obtaining the partial derivatives of all quantities at equilibrium for any pressure-based state specification. We applied the hybrid-EoS framework to isenthalpic and isentropic flashes involving water and illustrated its applicability using numerical benchmarks for water with light hydrocarbon and gas components. It can be concluded that, away from critical conditions of the aqueous phase but well within the conditions of interest for energy transition applications, the hybrid-EoS approach presents a robust, accurate and efficient modelling framework at any pressure-based state specification.

CRediT authorship contribution statement

M. Wapperom: Writing – original draft, Visualization, Validation, Software, Methodology, Data curation, Conceptualization. **J. Heringer:** Writing – review & editing, Software, Conceptualization. **D.V. Nichita:** Writing – review & editing, Supervision, Project administration, Funding acquisition. **D. Voskov:** Writing – review & editing, Supervision, Project administration, Funding acquisition, Conceptualization.

Declaration of competing interest

The authors declare that they have no known competing financial interests or personal relationships that could have appeared to influence the work reported in this paper.

Acknowledgement

We want to acknowledge the financial support of Michiel Wapperom and Juan Heringer by TotalEnergies.

Appendix A. Calculation of thermodynamic properties

Phase enthalpies, entropies and Gibbs free energies are calculated as the sum of an ideal and a residual part.

A.1. Ideal gas properties

To calculate the ideal gas contributions, only an expression of ideal gas heat capacities at constant volume or pressure is required, commonly expressed in simple power-series form (Passut and Danner, 1972):

$$C^*_{P,i}(T) = A + BT + CT^2 + DT^3 + ET^4 \tag{A.1}$$

The coefficients for (A.1) are given in Table A.2. Then, other properties can be obtained by applying thermodynamic relations. The ideal molar enthalpy:

$$\Delta H^*_i = \int_{T_0}^{T} C^*_{P,i}\, dT \tag{A.2}$$

The ideal molar entropy:

$$\Delta S^*_i = \int_{T_0}^{T} \frac{C^*_{P,i}}{T} dT - \int_{P_0}^{P} \frac{nR}{P} dP = \int_{T_0}^{T} \frac{C^*_{P,i}}{T} dT - nR \ln \frac{P}{P_0} \tag{A.3}$$

The ideal molar Gibbs free energy follows from the relation:

$$\Delta G^*_i = \Delta H^*_i - T\Delta S^*_i \tag{A.4}$$

The total ideal gas enthalpy is calculated by a summation over the mole numbers:

$$\Delta H^* = \sum_i n_i \Delta H^*_i \tag{A.5}$$

Total ideal gas entropy contains an additional term that results from (ideal) mixing:

$$\Delta S^* = \sum_i n_i \Delta S^*_i - R \sum_i n_i \ln x_i \tag{A.6}$$

Table A.2
Pure component ideal gas heat capacity coefficients for (A.1).

i	A/R	$B/R \cdot 10^2$	$C/R \cdot 10^5$	$D/R \cdot 10^9$
H_2O	3.8747	0.0231	0.1269	−0.4321
CO_2	2.6751	0.7188	−0.4208	0.8977
CH_4	2.3902	0.6039	0.1525	−1.3234
H_2S	3.5577	0.1574	0.0686	−0.3959
nC_5	0.8142	5.4598	−2.6997	5.0824

A.2. Residual properties

For an EoS with an expression for $P(V,T,\mathbf{n})$, residual enthalpy can be calculated by Mollerup and Michelsen (1992):

$$H^r(P,T,\mathbf{n}) = A^r(V,T,\mathbf{n}) + PV - nRT + T\left(\frac{\partial A^r}{\partial T}\right)_{V,\mathbf{n}} \tag{A.7}$$

Residual entropy:

$$S^r(P,T,\mathbf{n}) = \left(\frac{\partial A^r}{\partial T}\right)_{V,\mathbf{n}} + nR\ln Z \tag{A.8}$$

Equivalently, residual enthalpies can be obtained from partial derivatives of the fugacity or fugacity coefficient (Michelsen and Mollerup, 2007):

$$-\frac{H^r(P,T,\mathbf{n})}{T} = nRT\left(\frac{\partial \ln f_i}{\partial T}\right)_{P,\mathbf{n}} = nRT\left(\frac{\partial \ln \varphi_i}{\partial T}\right)_{P,\mathbf{n}} \tag{A.9}$$

This holds for the fugacity-activity model as well. Consequently, aqueous phase enthalpies can be calculated using the partial derivatives of solvent (6) and solutes (8) with respect to temperature.

Aqueous phase residual entropies can be obtained from the definition using enthalpy and Gibbs free energy:

$$S^r(P,T,\mathbf{n}) = (H^r(P,T,\mathbf{n}) - G^r(P,T,\mathbf{n}))/T \tag{A.10}$$

where $H^r(P,T,\mathbf{n})$ is obtained from (A.9) and Gibbs free energy is calculated from:

$$G^r(P,T,\mathbf{n}) = RT\sum_i n_{ij}\ln\varphi_{ij} \tag{A.11}$$

A.3. Partial derivatives of thermodynamic properties

For evaluating partial derivatives of primary and secondary properties at equilibrium, one needs to calculate the partial derivatives of the thermodynamic quantities with respect to their primary variables $X = \{P,T,\mathbf{n}\}$.

Partial derivatives of thermodynamic properties can be related to other thermodynamic quantities by means of partial derivatives of the PVT-relation (Michelsen and Mollerup, 2007):

$$\left(\frac{\partial H}{\partial P}\right)_{T,\mathbf{n}} = V - T\left(\frac{\partial V}{\partial T}\right)_{P,\mathbf{n}} \tag{A.12a}$$

$$\left(\frac{\partial H}{\partial T}\right)_{P,\mathbf{n}} = C_P^* + C_P^r \tag{A.12b}$$

$$\left(\frac{\partial S}{\partial P}\right)_{T,\mathbf{n}} = -\left(\frac{\partial V}{\partial T}\right)_{T,\mathbf{n}} \tag{A.12c}$$

$$\left(\frac{\partial S}{\partial T}\right)_{P,\mathbf{n}} = (C_P^* + C_P^r)/T \tag{A.12d}$$

where

$$C_P^r = C_V^r(V,T,\mathbf{n}) + T\left(\frac{\partial P}{\partial T}\right)_{V,\mathbf{n}}\left(\frac{\partial V}{\partial T}\right)_{P,\mathbf{n}} - nR \tag{A.12e}$$

$$C_V^r = -T\left(\frac{\partial^2 A^r}{\partial T^2}\right)_{V,\mathbf{n}} \tag{A.12f}$$

The partial derivatives of residual entropy, enthalpy and Gibbs free energy with respect to P and T are thus redundant and only the partial derivatives of the residual properties with respect to mole numbers are required. For instance:

$$\left(\frac{\partial S^r}{\partial n_k}\right)_{P,T,n_j\neq n_k} = \left(\frac{\partial^2 A^r}{\partial T\partial n_k}\right)_{V,n_j\neq n_k} + R\left[\ln Z + \frac{n}{Z}\left(\frac{\partial Z}{\partial n_k}\right)_{P,T,n_j\neq n_k}\right] \tag{A.13}$$

Such partial derivatives require careful implementation, as the expressions contain secondary properties (P, V, Z) that are a function of mole numbers. Partial derivatives of ideal gas properties with respect to n_k are trivial.

For fugacity models that are not explicitly formulated in terms of a pressure function, one cannot directly obtain partial derivatives of the PVT-relation and Helmholtz free energy expression. For such models, partial derivatives of the thermodynamic properties are obtained from the partial derivatives of ideal and residual parts. A look at the expressions for G^r, H^r and S^r indicates that this is trivial, provided the expressions for first- and second-order derivatives of $\ln\hat{\varphi}_i$ with respect to the primary variables P, T and n_k.

Note that for thermodynamic models that have mole fractions as a primary variable, rather than mole numbers, a chain rule is required to obtain the partial derivatives with respect to mole numbers:

$$\frac{\partial \ln\varphi_i}{\partial n_k} = \sum_m \frac{\partial \ln\varphi_i}{\partial x_m}\frac{\partial x_m}{\partial n_k} \tag{A.14}$$

Since $x_i = n_i/n_T$ and $n_T = \theta_j$, we can write

$$\frac{\partial x_i}{\partial n_k} = \frac{1}{\theta_j}(\delta_{ik} - x_i) \tag{A.15}$$

and the derivative of the fugacity coefficient with respect to mole numbers becomes

$$\frac{\partial \ln\varphi_i}{\partial n_k} = \frac{1}{\theta_j}\left(\frac{\partial \ln\varphi_i}{\partial x_k} - \sum_m x_m\frac{\partial \ln\varphi_i}{\partial x_m}\right) \tag{A.16}$$

Appendix B. Partial derivatives of phase equilibrium

To use gradient-based methods of the nested P-based phase equilibrium algorithm, evaluation of the partial derivatives of the PT-flash is required. Furthermore, in case the phase equilibrium calculations are integrated into a compositional flow and transport or process simulator, the partial derivatives of the flash procedure with respect to the primary variables in the simulation may be required. The partial derivatives can be obtained by implicit differentiation of the thermodynamic and material balance relations (2), (3) and (4), that comprise the multiphase isothermal–isobaric equilibrium procedure. The partial derivatives for isenthalpic and isentropic flashes can be calculated by applying the chain rule.

B.1. Derivatives of PT-flash

The thermodynamic and material balance relations read:

$$\ln\hat{f}_{ij}(T,P,\boldsymbol{n}_j) - \ln\hat{f}_{i0}(T,P,\boldsymbol{n}_0) = 0, \quad i = 1,\dots,n_c, \quad j = 1,\dots,n_p-1 \tag{2}$$

$$\sum_{j=0}^{n_p-1}\theta_j x_{ij} = z_i, \quad i = 1,\dots,n_c \tag{3}$$

$$\sum_{i=1}^{n_c}(x_{ij} - x_{i0}) = 0, \quad j = 1,\dots,n_p-1 \tag{4}$$

Together, these make up for $n_p(n_c+1)$ equations for the n_p phase fractions and $n_p n_c$ phase compositions. The primary variables of this set of equations are P, T and z_i.

Implicit differentiation of the fugacity relations with respect to state variable $\omega = \{P,T,z_k\}$ yields:

$$\frac{\partial \ln \varphi_{i0}}{\partial \omega_k}+\frac{1}{x_{i0}}\frac{\partial x_{i0}}{\partial \omega_k}-\frac{\partial \ln \varphi_{ij}}{\partial \omega_k}+\frac{1}{x_{ij}}\frac{\partial x_{ij}}{\partial \omega_k}=0,\quad i=1,\dots,n_c,\quad j=1,\dots,n_p-1 \tag{B.1}$$

The derivative of the fugacity coefficient is calculated by using the chain rule:

$$\frac{\partial \ln \varphi_{ij}}{\partial \omega_p}=\left(\frac{\partial \ln \varphi_{ij}}{\partial \omega_p}\right)_{\omega_k\neq\omega_p}+\sum_{k=1}^{n_c}\left(\frac{\partial \ln \varphi_{ij}}{\partial n_{kj}}\right)_{P,T}\frac{\partial n_{kj}}{\partial \omega_p} \tag{B.2}$$

where $\frac{\partial n_{ij}}{\partial \omega_k}=\frac{\partial \theta_j}{\partial \omega_k}x_{ij}+\frac{\partial x_{ij}}{\partial \omega_k}\theta_j$. The first term on the right hand side in (B.2) defaults to zero for partial derivatives with respect to overall composition z_k.

Implicit differentiation of the overall mass balance gives:

$$\sum_{j=0}^{n_p}\frac{\partial \theta_j}{\partial \omega_k}x_{ij}+\frac{\partial x_{ij}}{\partial \omega_k}\theta_j=\frac{\partial z_i}{\partial \omega_k},\quad i=1,\dots,n_c \tag{B.3}$$

where the right hand side equals zero for pressure and temperature derivatives, and

$$\frac{\partial z_i}{\partial z_k}=\begin{cases}1-z_i, & \text{if } i=k\\ -z_i, & \text{otherwise}\end{cases}$$

Finally, the contribution of the mole fraction relations (4) to the system of equations is:

$$\sum_{i=1}^{n_c}\left(\frac{\partial x_{i0}}{\partial \omega_k}-\frac{\partial x_{ij}}{\partial \omega_k}\right)=0,\quad j=1,\dots,n_p-1 \tag{B.4}$$

Following Nichita and Leibovici (2006), the expressions (B.2)–(B.3) can be reorganized such that the left-hand side of the system of equations is expressed as a set of linear combinations of all terms $\Delta\mathbf{n}=\{\Delta\mathbf{n_0}^T,\dots,\Delta\mathbf{n_{n_p-1}}^T\}$ making up system $\mathbf{J}\cdot\Delta\mathbf{n}=\mathbf{f}$:

$$\mathbf{J}=\begin{pmatrix}J_{A,00} & \cdots & J_{A,0n}\\ \vdots & \ddots & \vdots\\ J_{A,m0} & \cdots & J_{A,mn}\\ J_{Bi0} & \cdots & J_{Bin}\end{pmatrix} \tag{B.5a}$$

where A denotes the fugacity relation and B is the overall mole fraction relation.

$$J_{Aijk}=\frac{\partial \ln \hat{f}_{ij}}{\partial n_{kp}}-\frac{\partial \ln \hat{f}_{i0}}{\partial n_{kp}} \tag{B.5b}$$

$$J_{Bij}=\frac{\partial n_{ij}}{\partial n_{kp}} \tag{B.5c}$$

The right-hand side:

$$\mathbf{f}=\begin{pmatrix}f_A\\ f_B\end{pmatrix} \tag{B.6a}$$

$$f_{Aij}=\frac{\partial \ln \hat{f}_{ij}}{\partial \omega_k}-\frac{\partial \ln \hat{f}_{i0}}{\partial \omega_k} \tag{B.6b}$$

$$f_{Bi}=\frac{\partial z_i}{\partial \omega_k} \tag{B.6c}$$

For pressure and temperature derivatives, this comprises vector f where $f_{Bi}=0$ and for composition, it is matrix $\mathbf{F}$ with $F_{jk}=\frac{\partial F_j}{\partial z_k}$. This matrix contains mostly zeros as $F_{Aij}=0$.

Using this approach to obtain the derivatives for a PT-flash, we can solve partial derivatives of the flash using same matrix $\mathbf{A}$ irrespective of which set of partial derivatives with respect to P, T or z_k is chosen.

B.1.1. Derivatives of secondary properties for PT-flash

The derivative $\left(\frac{\partial M}{\partial \omega_k}\right)_{\omega_j\neq\omega_k}$ of any secondary property M at equilibrium with respect to any of the primary PT-flash variables $\omega=\{P,T,\mathbf{z}\}$ can be formulated by means of a chain rule of the primary variables of the property $\psi=\{P,T,\mathbf{n}\}$:

$$\left(\frac{\partial M}{\partial \omega_p}\right)_{\omega_j\neq\omega_p}=\left(\frac{\partial M}{\partial \omega_p}\right)_{\psi_j\neq\omega_p}+\sum_k\left(\frac{\partial M}{\partial n_k}\right)_{P,T,n_j\neq n_k}\left(\frac{\partial n_k}{\partial \omega_p}\right)_{\omega_j\neq\omega_p} \tag{B.7}$$

The first term vanishes for any derivatives with respect to z_k as it is not a primary variable for the property calculation. The summation term reflects the dependency of the property to composition changes and therefore involves derivatives of the flash.

Evaluation of $g'(T)$ of the specific Q-function with respect to temperature requires the derivatives of the PT-flash procedure:

$$\left(\frac{\partial H}{\partial T}\right)_{P,\mathbf{z}}=\left(\frac{\partial}{\partial T}\sum_j H_j\right)_{P,\mathbf{z}}=\sum_j\left(\left(\frac{\partial H_j}{\partial T}\right)_{P,\mathbf{n}_j}+\sum_i\left(\frac{\partial H_j}{\partial n_{ij}}\right)_{P,T,n_k}\frac{\partial n_{ij}}{\partial T}\right) \tag{B.8a}$$

$$\left(\frac{\partial S}{\partial T}\right)_{P,\mathbf{z}}=\left(\frac{\partial}{\partial T}\sum_j S_j\right)_{P,\mathbf{z}}=\sum_j\left(\left(\frac{\partial S_j}{\partial T}\right)_{P,\mathbf{n}_j}+\sum_i\left(\frac{\partial S_j}{\partial n_{ij}}\right)_{P,T,n_k}\frac{\partial n_{ij}}{\partial T}\right) \tag{B.8b}$$

The partial derivatives of phase enthalpies and entropies have been described in Appendix A.

B.2. Derivatives of PH- and PS-flash

B.2.1. Away from transition temperatures

The partial derivatives of the primary quantities of isenthalpic and isentropic phase equilibrium calculations with respect to primary variables ψ, as well as any secondary properties, can be calculated by applying the chain rule to the PT-results ω:

$$\left(\frac{\partial M}{\partial \psi_k}\right)_{\psi_j\neq\psi_k}=\left(\frac{\partial M}{\partial \omega_k}\right)_{\omega_j\neq\omega_k}+\left(\frac{\partial M}{\partial T}\right)_{P,T,\mathbf{z}}\left(\frac{\partial T}{\partial \psi_k}\right)_{\psi_j\neq\psi_k} \tag{B.9}$$

For this, one needs to calculate the derivative of temperature T with respect to the primary variable of the PH- or PS-flash ψ: $\left(\frac{\partial T}{\partial \psi_k}\right)_{\psi_j\neq\psi_k}$. For any function $F(x,y,z)=0$, the following relationship between the partial derivatives holds:

$$\left(\frac{\partial z}{\partial x}\right)_y\left(\frac{\partial x}{\partial y}\right)_z\left(\frac{\partial y}{\partial z}\right)_x=-1 \tag{B.10}$$

Consequently, one can formulate the function $F(P,T,X,\mathbf{z})=0$ with $X=\{H,S\}$ and use the relationship in (B.10) to obtain the partial derivatives required for the chain rule (B.9). For instance:

$$\left(\frac{\partial T}{\partial P}\right)_{H,\mathbf{z}}=-\left(\frac{\partial H}{\partial P}\right)_{T,\mathbf{z}}\Big/\left(\frac{\partial H}{\partial T}\right)_{P,\mathbf{z}} \tag{B.11}$$

B.2.2. At transition temperatures

At a transition temperature, the phase split is described by (14a). As described by Sun et al. (2017), one needs to find the partial derivatives of the weighted flash results M (14a) with respect to the primary flash variables ψ to obtain the derivatives of the isenthalpic or isentropic flash at transition temperatures:

$$\left(\frac{\partial M}{\partial \psi_k}\right)_{\psi_j\neq\psi_k}=\beta\left(\frac{\partial M^a}{\partial \psi_k}\right)_{\psi_j\neq\psi_k}+(1-\beta)\left(\frac{\partial M^b}{\partial \psi_k}\right)_{\psi_j\neq\psi_k}+(M^a-M^b)\left(\frac{\partial \beta}{\partial \psi_k}\right)_{\psi_j\neq\psi_k} \tag{B.12}$$

In the partial derivatives of flashes at a and b, the derivative of temperature with respect to the primary variables in (B.9) is replaced by the partial derivative of the transition temperature. This partial derivative is obtained by evaluating the sensitivity of the equilibrium conditions (13):

$$\left(\frac{\partial T}{\partial \omega_k}\right)_{\omega_j\neq\omega_k}=-\left[\frac{\partial G^a-G^b}{\partial \omega_k}\right]_{\omega_j\neq\omega_k}\Big/\left[\frac{\partial G^a-G^b}{\partial T}\right]_{P,\mathbf{z}} \tag{B.13}$$

In addition, the partial derivatives of the weight β with respect to the primary variables ψ are required:

$$\left(\frac{\partial \beta}{\partial \psi_k}\right)_{\psi_j\neq\psi_k}=-\frac{1}{X^a-X^b}\left[\beta\left(\frac{\partial X^a}{\partial \psi_k}\right)_{\psi_j\neq\psi_k}+(1-\beta)\left(\frac{\partial X^b}{\partial \psi_k}\right)_{\psi_j\neq\psi_k}\right] \tag{B.14}$$

where the partial derivatives of X^a and X^b are also obtained by applying the chain rule:

$$\left(\frac{\partial X^a}{\partial \psi_k}\right)_{\psi_j \neq \psi_k} = \left(\frac{\partial X^a}{\partial \psi_k}\right)_{\omega_j \neq \psi_k} + \left(\frac{\partial X^a}{\partial T}\right)_{P,\mathbf{z}} \left(\frac{\partial T}{\partial \psi_k}\right)_{\psi_j \neq \psi_k} \tag{B.15}$$

Data availability

Data will be made available on request.

References

Soave, G., 1972. Equilibrium constants from a modified redlich-kwong equation of state. Chem. Eng. Sci. 27, 1197–1203.

Peng, D.-Y., Robinson, D.B., 1976. A new two-constant equation of state. Ind. Eng. Chem. Fundam. 15 (1), 59–64.

Søreide, I., Whitson, C.H., 1992. Peng-robinson predictions for hydrocarbons, CO_2, N_2, and H_2S with pure water and NaCl brine. Fluid Phase Equilib. 77, 217–240.

Michel, S., Hooper, H.H., Prausnitz, J.M., 1989. Mutual solubilities of water and hydrocarbons from an equation of state. Need for an unconventional mixing rule. Fluid Phase Equilib. 45 (2–3), 173–189.

Chapman, W.G., Gubbins, K.E., Jackson, G., Radosz, M., 1989. SAFT: Equation-of-state solution model for associating fluids. Fluid Phase Equilib. 52, 31–38.

Kontogeorgis, G.M., Voutsas, E.C., Yakoumis, I.V., Tassios, D.P., 1996. An equation of state for associating fluids. Ind. Eng. Chem. Res. 35 (11), 4310–4318.

Michelsen, M.L., Hendriks, E.M., 2001. Physical properties from association models. Fluid Phase Equilib. 180 (1–2), 165–174.

Li, Y.-K., Nghiem, L.X., 1986. Phase equilibria of oil, gas and water/brine mixtures from a cubic equation of state and Henry's law. Can. J. Chem. Eng. 64 (3), 486–496.

Ziabakhsh-Ganji, Z., Kooi, H., 2012. An equation of state for thermodynamic equilibrium of gas mixtures and brines to allow simulation of the effects of impurities in subsurface CO_2 storage. Int. J. Greenh. Gas Control. 11S, S21–S34.

Akinfiev, N.N., Diamond, L.W., 2003. Thermodynamic description of aqueous non-electrolytes at infinite dilution over a wide range of state parameters. Geochim. Cosmochim. Acta 67 (4), 613–629.

Duan, Z., Møller, N., Greenberg, J., Weare, J.H., 1992. The prediction of methane solubility in natural waters to high ionic strength from 0 to 250 °C and from 0 to 1600 bar. Geochim. Cosmochim. Acta 56 (4), 1451–1460.

Pitzer, K.S., 1973. Thermodynamics of electrolytes. I. Theoretical basis and general equations. J. Phys. Chem. 77 (2), 268–277.

Jager, M.D., Ballard, A.L., Sloan, Jr, E.D., 2003. The next generation of hydrate prediction II. Dedicated aqueous phase fugacity model for hydrate prediction. Fluid Phase Equilib. 211, 85–107.

Wapperom, M., Taghinejad, S.M., Lyu, X., Farajzadeh, R., Voskov, D., 2026. A thermodynamically consistent simulation of gas hydrates in porous media using operator-based linearization. Energy Convers. Manag.: X 30.

Nichita, D.V., 2024. A unified presentation of phase stability analysis including all major specifications. Fluid Phase Equilib. 578, 113990.

Paterson, D., Yan, W., Michelsen, M.L., Stenby, E.H., 2019. Multiphase isenthalpic flash: General approach and its adaptation to thermal recovery of heavy oil. Adv. Chem. Eng. 65 (1), 281–293.

Moncorgé, A., Petitfrère, M., Thibeau, S., 2022. Complete equation of state thermal formulation for simulation of CO_2 storage. SPE J. 27 (1), 914–928.

Castier, M., Kanes, R., Véchot, L.N., 2015. Flash calculations with specified entropy and stagnation enthalpy. Fluid Phase Equilib. 408, 196–204.

Michelsen, M.L., 1987. Multiphase isenthalpic and isentropic flash algorithms. Fluid Phase Equilib. 33, 13–27.

Agarwal, R., Li, Y., Nghiem, L., Coombe, D., 1991. Multiphase multicomponent isenthalpic flash calculations. J. Can. Pet. Technol. 30 (03), 69–75.

Baker, L.E., Pierce, A.C., Luks, K.D., 1982. Gibbs energy analysis of phase equilibria. SPE J. 22 (5), 731–742.

Iranshahr, A., Voskov, D., Tchelepi, H., 2012. Gibbs energy analysis: Compositional tie-simplex space. Fluid Phase Equilib. 321, 49–58.

Michelsen, M.L., 1982a. The isothermal flash problem. Part I. Stability. Fluid Phase Equilib. 9, 1–19.

Nichita, D.V., Leibovici, C.F., 2013. A rapid and robust method for solving the rachford–rice equation using convex transformations. Fluid Phase Equilib. 353, 38–49.

Michelsen, M.L., 1994. Calculation of multiphase equilibrium. Comput. Chem. Eng. 18 (7), 545–550.

Leibovici, C.F., Nichita, D.V., 2008. A new look at multiphase rachford–rice equations for negative flashes. Fluid Phase Equilib. 267, 127–132.

Yan, W., Stenby, E.H., 2012. On multiphase negative flash for ideal solutions. Fluid Phase Equilib. 322–323, 41–47.

Petitfrere, M., Nichita, D., 2015a. A comparison of conventional and reduction approaches for phase equilibrium calculations. Fluid Phase Equilib. 386, 30–46.

Petitfrere, M., Nichita, D., 2015b. Multiphase equilibrium calculations using a reduction method. Fluid Phase Equilib. 401, 110–126.

Michelsen, M.L., Mollerup, J.M., 1986. Partial derivatives of thermodynamic properties. AIChE J. 32 (8), 1389–1392.

Mollerup, J.M., Michelsen, M.L., 1992. Calculation of thermodynamic equilibrium properties. Fluid Phase Equilib. 74, 1–15.

Iranshahr, A., Voskov, D., Tchelepi, H., 2013a. A negative-flash tie-simplex approach for multiphase reservoir simulation. SPE J. 18 (6), 1140–1149.

Whitson, C.H., Michelsen, M.L., 1989. The negative flash. Fluid Phase Equilib. 53, 51–71.

Leibovici, C.F., Neoschil, J., 1995. A solution of rachford-rice equations for multiphase systems. Fluid Phase Equilib. 112, 217–221.

Iranshahr, A., Voskov, D., Tchelepi, H.A., 2010. Generalized negative-flash method for multiphase multicomponent systems. Fluid Phase Equilib. 299, 272–284.

Iranshahr, A., Voskov, D., Tchelepi, H., 2013b. Tie-simplex based compositional space parameterization: Continuity and generalization to multiphase systems. AIChE J. 59 (5), 1684–1701.

Imre, A.R., Kraska, T., 2005. Stability limits in binary fluids mixtures. J. Chem. Phys. 122, 064507.

Kamath, R.S., Biegler, L.T., Grossmann, I.E., 2010. An equation-oriented approach for handling thermodynamics based on cubic equation of state in process optimization. Comput. Chem. Eng. 34, 2085–2096.

Michelsen, M.L., 1982b. The isothermal flash problem. Part II. Phase split calculation. Fluid Phase Equilib. 9, 21–40.

Tödheide, K., Franck, E.U., 1963. Das zweiphasengebiet und die kritische kurve im system kohlendioxid–wasser bis zu drucken von 3500 bar. Z. Für Phys. Chem. 37 (5–6), 387–401.

Dhima, A., de Hemptinne, J.-C., Jose, J., 1999. Solubility of hydrocarbons and CO_2 mixtures in water under high pressure. Ind. Eng. Chem. Res. 38 (8), 3144–3161.

Qin, J., Rosenbauer, R.J., Duan, Z., 2008. Experimental measurements of vapor-liquid equilibria of the H_2O+CO_2+CH_4 ternary system. J. Chem. Eng. Data 53 (6), 1246–1249.

Huang, S.S.-S., Leu, A.-D., Ng, H.-J., Robinson, D.B., 1985. The phase behavior of two mixtures of methane, carbon dioxide, hydrogen sulfide, and water. Fluid Phase Equilib. 19 (1–2), 21–32.

Savary, V., Berger, G., Dubois, M., Lacharpagne, J.-C., Pages, A., Thibeau, S., Lescanne, M., 2012. The solubility of CO_2+H_2S mixtures in water and 2 M NaCl at 120 °C and pressures up to 35 MPa. Int. J. Greenh. Gas Control. 10, 123–133.

Michelsen, M.L., 1999. State function based flash specifications. Fluid Phase Equilib. 158–160, 617–626.

Xu, L., Moncorgé, A., Nichita, D.V., 2025. Efficient nested three-phase isenthalpic flash calculations with a hybrid Newton and brent algorithm for water-CO_2-hydrocarbon mixtures in CO_2 storage simulations. Chem. Eng. Sci. 308, 121379.

Pitzer, K.S., Peiper, J.C., Busey, R.H., 1984. Thermodynamic properties of aqueous sodium chloride solutions. J. Phys. Chem. Ref. Data 13 (1), 1–102.

Koschel, D., Coxam, J.-Y., Rodier, L., Majer, V., 2006. Enthalpy and solubility data of CO_2 in water and NaCl (aq) at conditions of interest for geological sequestration. Fluid Phase Equilib. 247, 107–120.

Chen, X., Gillespie, S.E., Oscarson, J.L., Izatt, R.M., 1992. Calorimetric determination of thermodynamic quantities for chemical reactions in the system CO_2-NaOH-H_2O from 225 to 325°C. J. Solut. Chem. 21, 825–848.

Sun, H., Raghavan, A., Haugen, K., Chempath, S., 2017. An improved isenthalpic flash algorithm based on maximization of entropy. Fluid Phase Equilib. 438, 18–28.

Brent, R.P., 1971. An algorithm with guaranteed convergence for finding a zero of a function. Comput. J. 14 (4), 422–425.

Wagner, W., Pruß, A., 2002. The IAPWS formulation 1995 for the thermodynamic properties of ordinary water substance for general and scientific use. J. Phys. Chem. Ref. Data 31, 387–535.

Di Zhu, Okuno, R., 2015. Robust isenthalpic flash for multiphase water/hydrocarbon mixtures. SPE J. 20 (6), 1350–1365.

Passut, C.A., Danner, R.P., 1972. Correlation of ideal gas enthalpy, heat capacity and entropy. Ind. Eng. Chem. Process. Des. Dev. 11 (4), 543–546.

Michelsen, M.L., Mollerup, J.M., 2007. Thermodynamic Models: Fundamentals & Computational Aspects, second ed. Tie-Line Publications, Holte, Denmark.

Nichita, D.V., Leibovici, C.F., 2006. Calculation of joule–thomson inversion curves for two-phase mixtures. Fluid Phase Equilib. 246 (1–2), 167–176.